



Direct numerical simulation of a temporally-developing subsonic round jet and its sound field

Christophe Bogey*

Laboratoire de Mécanique des Fluides et d'Acoustique

UMR CNRS 5509, Ecole Centrale de Lyon

69134 Ecully, France

A temporally-developing isothermal round jet at a Mach number of 0.9 and a diameter-based Reynolds number of 3125 is computed by direct numerical simulations in order to investigate its turbulent development and its generated noise. The simulations are performed using high-order finite differences on a grid of 940 million points extending up to 120 jet radii in the axial direction. Snapshots and statistical properties of the jet flow and acoustic fields are shown. The latter are calculated from five runs using different initial random perturbations in the jet shear layers. They include mean, rms, skewness and kurtosis values and auto-correlations of flow velocity and near-field pressure, as well as flow-noise cross-covariances. It is found that, when the jet potential core closes, mixing-layer turbulent structures intermittently intrude, accelerate and merge on the jet axis. Simultaneously, strong low-frequency acoustic waves, significantly correlated with the centerline flow fluctuations, are emitted in the downstream direction. The present results for a temporally-developing jet are very similar to those obtained at the end of the potential core in spatially-developing jets. This suggests the presence in both cases of the same sound source on the jet axis due to the potential-core closing, radiating mainly in the downstream direction.

I. Introduction

For more than fifty years of research, there have been significant progress in the understanding of noise generation in subsonic jets. The source distribution along the axial direction in the jets was shown, using source localization techniques as in Chu & Kaplan¹ and Fisher *et al.*² and more recently in Lee & Bridges³ for instance, to depend on the Strouhal number $St_D = fD/u_j$, where f is the frequency, and D and u_j are the jet diameter and velocity. Overall, high-frequency sound sources are located near the nozzle exit, whereas low-frequency sources lie in the vicinity of the end of the jet potential core. The sound spectra measured in the acoustic field were also found to be dominated by low-frequency components in the downstream direction, but to be broadband in the sideline and upstream directions, see the far-field measurements of Mollo-Christensen *et al.*⁴ for example. These observations, and other experimental and numerical findings reported in Tam,⁵ Panda *et al.*⁶ and Tam *et al.*,⁷ and in Bogey *et al.*⁸ and Bogey & Bailly,^{9,10} among others, suggested the presence of two jet noise components, namely a low-frequency downstream component and a broadband component with a relatively uniform directivity. Thanks notably to the work of Tam & Auriault,¹¹ the broadband component was identified as the noise of the fine-scale turbulence of the jet flow. The low-frequency component, typically centered around $St_D = 0.2$, was attributed to the large-scale flow structures. It appears to be produced at the end of the jet potential core where the turbulent shear layers merge, and flow intermittency is strong. Unfortunately, the corresponding noise generation mechanism is still not clearly understood.

In order to isolate and characterize that sound source, it can be worth not considering the full jet, but a model of the jet flow. One possibility is to conduct analyses of the jet instability waves, as done in Tam & Morris¹² and Crighton & Huerre,¹³ just to mention a few well-known pioneers in that field. Another is to

*CNRS Research Scientist, AIAA Senior Member & Associate Fellow, christophe.bogey@ec-lyon.fr

perform simulations of a reduced or simplified jet flow configuration. This is the case in the present work in which a temporally-developing subsonic round jet is computed. In the past, temporal simulations have been performed for fully developed channel and pipe flows, and turbulent boundary layers, e.g. in Kim *et al.*,¹⁴ Eggels *et al.*¹⁵ and Kozul *et al.*¹⁶ Temporally-developing planar mixing layers have been calculated in several studies, including those by Comte *et al.*,¹⁷ Rogers & Moser,¹⁸ Vreman *et al.*¹⁹ and Freund *et al.*,^{20,21} in order to describe the turbulent development and the compressibility effects in free shear flows. Simulations of temporal planar mixing layers have also enabled researchers to study noise generation in such flows, refer to Fortuné *et al.*²² and Kleimann & Freund²³ for subsonic mixing layers, and to Anderson & Freund,²⁴ Buchta *et al.*^{25,25} and Terakado *et al.*²⁷ for supersonic mixing layers. Computations of temporally-developing jets, such as those by van Reeuwijk & Holzner²⁸ for a planar jet and by Hawkes *et al.*²⁹ for a plane jet flame, are much less numerous. This is certainly because temporal jets do not exit from a nozzle, and have a potential core of infinite length, which renders the comparisons with spatially-developing jets difficult. As a model, however, they can be expected to provide information on the physics of jet flows, which should allow us to discuss the validity of theories on these flows.

In the present work, a temporally-developing isothermal round jet at a Mach number of 0.9 and a diameter-based Reynolds number of 3125 is computed using direct numerical simulation (DNS) in order to investigate its turbulent development and its generated sound field. With this aim in view, the main statistical properties of the jet velocity and near pressure fields are presented, and velocity and pressure correlations are calculated in order to estimate the convection velocity of the turbulent structures in the jet and the radiation angle of the acoustic waves outside. Cross-covariances between flow quantities on the jet axis and near-field pressure are also estimated to track causal links between potential sources and observer. The main objective of this study is to determine whether the temporal jet generates sound waves in the same way as spatially-developing subsonic jets, notably the jets of Stromberg *et al.*,³⁰ Freund³¹ and Bogey & Bailly^{9,10} at similar low Reynolds numbers. The particular question that arises and needs to be answered here is whether, when the shear layers of the temporal jet merge, low-frequency waves are emitted in the downstream direction as happens at the end of the potential core of spatially-developing jets. If so, this will suggest that they are produced by the same noise generation mechanism, independently of the presence of a nozzle or of a potential core of finite length.

The paper is organized as follows. The main characteristics of the jet and of the simulations, including initial conditions, numerical methods, grid and computational parameters, are documented in section II. The simulation results, namely vorticity and pressure snapshots, the main characteristics of the jet flow and near acoustic fields, and flow-noise cross-correlations, are presented in section III. Finally, concluding remarks are given in section IV.

II. Parameters

A. Jet definition

The jet is round and isothermal, and is characterized by a Mach number of $M = u_j/c = 0.9$ and a Reynolds number of $Re_D = u_j D/\nu = 3125$, where u_j and $D = 2r_0$ are the jet initial centerline velocity and diameter, and c and ν are the speed of sound and kinematic molecular viscosity. The ambient temperature and pressure are $T_a = 293$ K and $p_a = 10^5$ Pa. At initial time $t = 0$, the hyperbolic-tangent profile of axial velocity presented in figure 1(a) is considered. The momentum thickness of the mixing layer is set to $\delta_\theta = 2r_0/\sqrt{Re_D} = 0.0358r_0$, following the variations of δ_θ/r_0 with the Reynolds number observed in experiments for initially laminar jets, e.g. in Zaman.³² This leads to a momentum Reynolds number of $Re_\theta = u_j \delta_\theta/\nu = 56$. Radial and azimuthal velocities are set to zero, pressure is equal to p_a , and density is determined by a Crocco-Busemann relation.

At $t = 0$, velocity perturbations of low amplitude are added in the mixing layers in order to seed the laminar-turbulent transition. For this, as proposed in Bogey *et al.*,⁸ divergence-free Gaussian ring vortices of radius r_0 are imposed. These vortices have a half-width of $2\delta_\theta$, and are regularly distributed in the axial direction every $\Delta z = 0.025r_0$, where Δz is the axial mesh spacing. At each position, the vortex has a maximum velocity randomly fixed between 0 and $0.01u_j$, and is weighted in the azimuthal direction by the function $\cos(n_\theta\theta + \varphi)$ where n_θ and φ are randomly chosen between 0 and 32 and between 0 and 2π , respectively. This allows a peak turbulence intensity of about 1% to be reached at $t = 0$. Finally, note that five runs of the simulation are performed using different random seeds in order to obtain better converged statistical results.

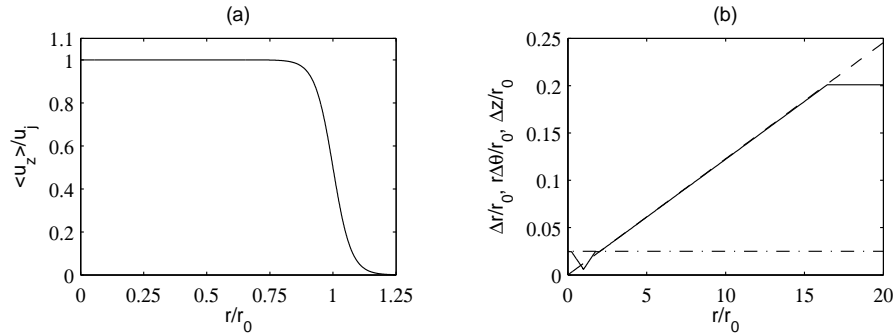


Figure 1. Radial profiles of (a) the axial velocity $\langle u_z \rangle / u_j$ at $t = 0$, and (b) the radial, azimuthal and axial mesh spacings — $\Delta r/r_0$, — — — $r\Delta\theta/r_0$ and — · — · $\Delta z/r_0$.

B. Numerical methods

The numerical framework is identical to that used in recent simulations of round jets.^{33–36} The simulations are carried out using an in-house solver of the three-dimensional filtered compressible Navier-Stokes equations in cylindrical coordinates (r, θ, z) based on low-dissipation and low-dispersion, high-order explicit schemes. The axis singularity is taken into account by the method of Mohseni & Colonius.³⁷ In order to alleviate the time-step restriction near the cylindrical origin, the derivatives in the azimuthal direction around the axis are calculated at coarser resolutions than permitted by the grid.³⁸ For the points closest to the jet axis, they are evaluated using 16 points, yielding an effective resolution of $2\pi/16$. Fourth-order eleven-point centered finite differences are used for spatial discretization, and a second-order six-stage Runge-Kutta algorithm is implemented for time integration.³⁹ A twelfth-order eleven-point centered filter is applied explicitly to the flow variables every time step in order to remove grid-to-grid oscillations while leaving larger scales mostly unaffected. Non-centered finite differences and filters are also used near the grid boundaries.^{33,40} The radiation conditions of Tam & Dong^{41,42} are applied at the sideline boundaries to avoid significant acoustic reflections. Obviously, since a temporally-developing flow is considered, periodic boundary conditions are imposed in the axial direction.

C. Simulation parameters

The mesh grid used in the different runs extends up to $z = 120r_0$ in the axial direction, and out to $r = 30r_0$ in the radial direction. It contains $n_r \times n_\theta \times n_z = 382 \times 512 \times 4800 = 940$ million points. The mesh spacing in the axial direction is uniform and equal to $\Delta z = 0.025r_0$, whereas, as illustrated in figure 1(b), the mesh spacing in the radial direction varies. The latter is minimum and equal to $\Delta r = 0.006r_0$ at $r = r_0$. It is maximum and equal to $\Delta r = 0.2r_0$ for $r \geq 16r_0$, yielding a Strouhal number of $St_D = 2.8$ for an acoustic wave discretized by four points per wavelength. The use of $n_\theta = 512$ points in the azimuthal direction leads to $r\Delta\theta = 0.012r_0$ at $r = r_0$. Note that the simulations have been checked to be fully-resolved DNS from the calculation of the turbulent kinetic energy budgets.

The computations are performed using an OpenMP-based in-house solver on 32-core nodes of Intel E5-4650 processors with a clock speed of 2.7 GHz and 16-core nodes of Intel E5-2670 processors at 2.6 GHz. The total number of iterations is equal to 22,400 in each run allowing a final time of $t = 75r_0/u_j$ to be reached. The time step Δt is chosen so that $\Delta t = 0.6\Delta r(r = r_0)/c$, ensuring the stability of the explicit time integration. For the present grid of about one billion points, 200 GB of memory are required, and about 1,000 CPU hours are consumed for 1,000 iterations. Density, the three velocity components, pressure and vorticity norm are recorded on the jet axis at $r = 0$ and on the cylindrical surfaces at $r = r_0, 4r_0$ and $20r_0$, at a sampling frequency allowing spectra to be computed up to $St_D = 10$, and on the four azimuthal planes at $\theta = 0, \pi/2, \pi$ and $3\pi/2$, at half the frequency mentioned above. The statistical results obtained in each run are averaged over the periodic directions z and θ . The results of the five runs are then ensemble averaged, providing mean values, denoted by $\langle \cdot \rangle$ in what follows, calculated over a distance of $600r_0$ in the streamwise direction.

III. Results

A. Vorticity and pressure snapshots

Snapshots of the vorticity norm obtained in the plane (r, z) at $\theta = 0$ and $\theta = \pi$ at the seven times $tu_j/r_0 = 10, 15, 20, 25, 30, 35$ and 40 are represented in figure 2. At the first time, the mixing layers exhibit small oscillations due to the growth of instability waves in the hyperbolic-tangent velocity profile.⁴³ Later, they roll up, and vortices of size typically equal to the shear-layer thickness are formed. These vortices then grow thanks to the pairing mechanism,⁴⁴ and start to interact across the jet potential core at $tu_j/r_0 = 20$. They appear to merge on the centerline at $tu_j/r_0 = 25$, resulting in the disappearance of the potential core. Finally, for $tu_j/r_0 \geq 30$, the jet is developed, and contains vortical structures of decreasing intensity and increasing size with time.

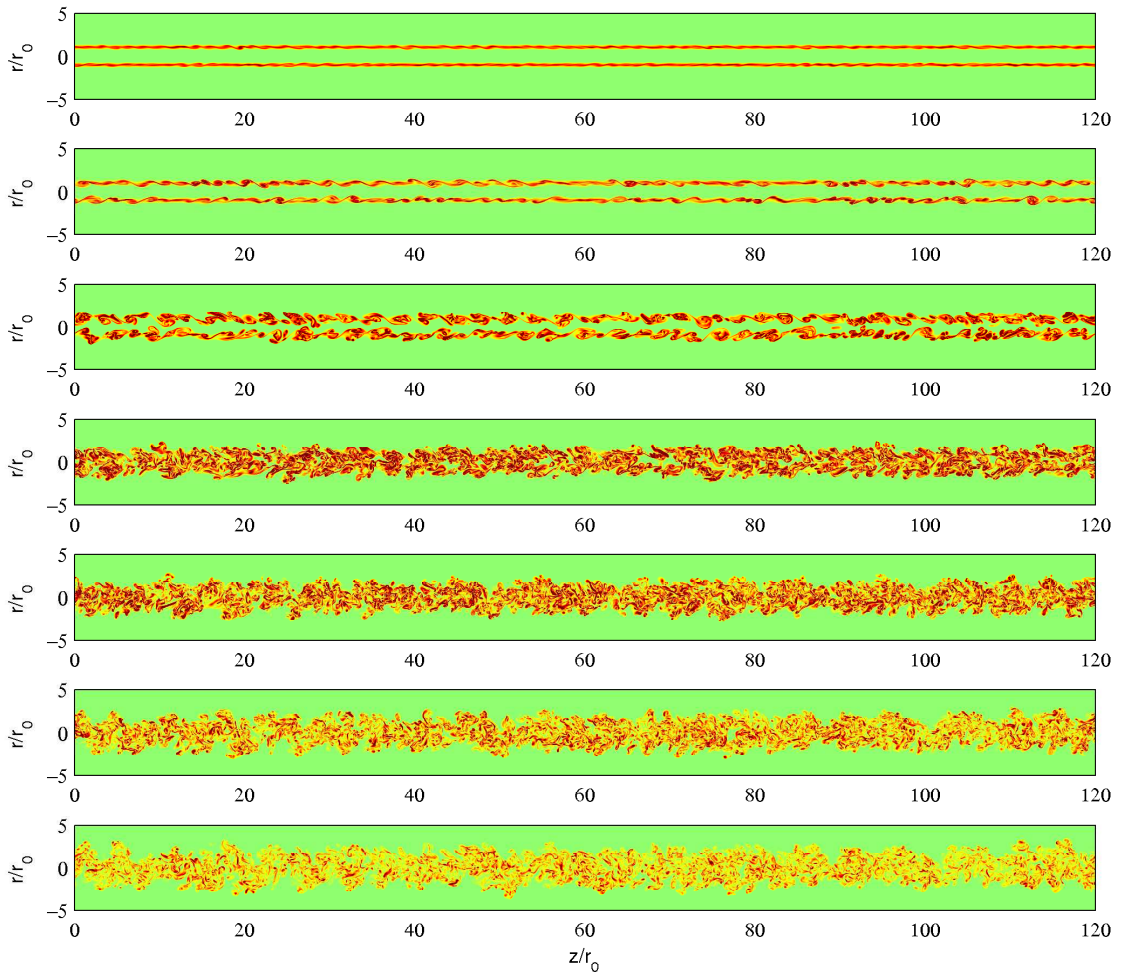


Figure 2. Representation of vorticity norm obtained at $tu_j/r_0 = 10, 15, 20, 25, 30, 35$ and 40 , from top to bottom. The color scale ranges up to the level of $4u_j/r_0$.

Snapshots of the vorticity norm and pressure obtained respectively inside and outside of the flow at $tu_j/r_0 = 20, 30, 40$ and 50 in the plane (r, z) are provided in figure 3. At $tu_j/r_0 = 20$, just before the potential-core closing, high-amplitude waves, showing alternatively positive and negative pressure fluctuations, are observed in the immediate vicinity of the jet. They are most likely hydrodynamic pressure waves associated with the coherent structures of the jet flow.^{45,46} At $tu_j/r_0 = 30$, after the shear-layer merging, strong waves are seen in the acoustic near field up to $r \simeq 10r_0$. They appear to be symmetric with respect to the jet centerline, and to have a typical wavelength of about $15r_0$. Moreover, they seem to propagate mainly in the downstream direction. At $tu_j/r_0 = 40$ and 55 , they are still well visible, supporting their downstream directivity. They also have a very large spatial extent along the wave front direction. Interestingly, they look like the waves emitted at shallow angles by spatially-developing subsonic jets.^{8,9}

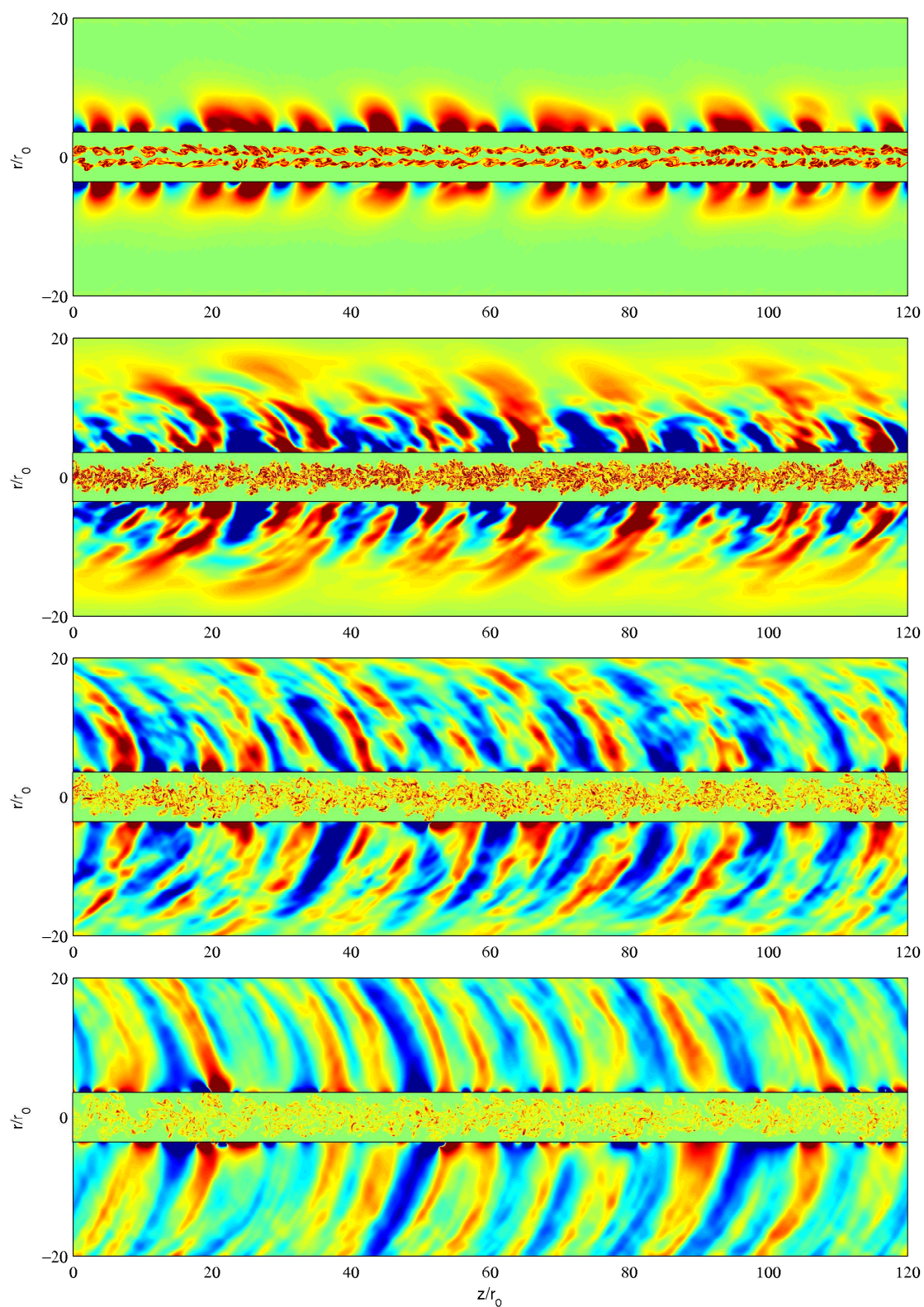


Figure 3. Representation of vorticity norm inside the jet flow and of pressure fluctuations outside, obtained at $tu_j/r_0 = 20, 30, 40$ and 50 , from top to bottom. The color scales range up to the level of $4u_j/r_0$ for vorticity, and from -200 Pa to 200 Pa for pressure.

B. Statistical properties of velocity and pressure fields

The mean and rms values of axial velocity and pressure calculated for the jet are represented in figure 4 using (t, r) coordinates. The results bear striking similarities with the flow and near sound fields measured in the (z, r) plane of spatially-developing subsonic jets.^{47–49} The mean axial velocity field of figure 4(a) shows the jet spreading with time, and indicates, based on the contour line of $0.95u_j$, that the jet potential core closes at time $t_c u_j / r_0 = 21.5$. In parallel to the mean flow development, the axial turbulence intensity is found in figure 4(b) to grow in the jet shear layer, to reach values slightly higher than 20% between $tu_j / r_0 = 20.5$ and 23.5, and then to decrease. As for the mean pressure field of figure 4(c), with respect to the ambient pressure, negative values are obtained in the jet flow as usually encountered in turbulent flows. Two regions of weak positive values are also visible in the jet near field just after $t = 0$ and after $tu_j / r_0 \simeq 14r_0$. They most likely result from transient cylindrical acoustic waves due to the flow initial conditions and the shear-layer rolling-up. Finally, the rms pressure field of figure 4(d) reveals that noise is generated in the jet around $tu_j / r_0 \simeq 20$, and propagates outside with increasing time.

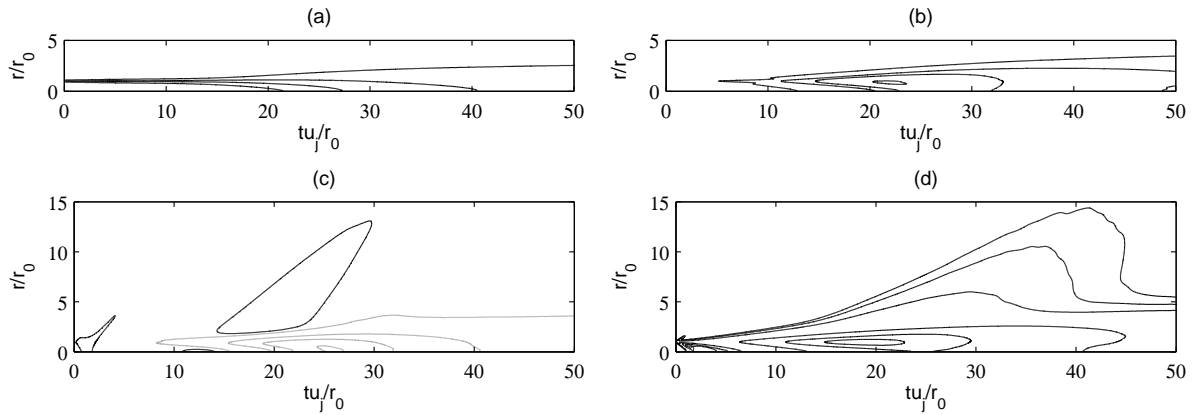


Figure 4. Space-time representation of the mean and rms fields of (top) axial velocity and (bottom) pressure using the contour line values of: (a) $\langle u_z \rangle / u_j = 0.05, 0.35, 0.65$ and 0.95 , (b) $\langle u'_z u'_z \rangle^{1/2} / u_j = 0.02, 0.08, 0.14$ and 0.20 , (c) $\langle p \rangle - p_a = -3000, -2000, -1000$ and -50 Pa (grey) and 50 Pa (black), and (d) $\langle p' p' \rangle^{1/2} = 60, 80, 140, 1000, 3000$ and 5000 Pa.

The time variations of the shear-layer momentum thickness δ_θ , of the mean centerline axial velocity, and of the peak value of axial turbulence intensity are plotted in figure 5. In figure 5(a), the shear layer is noted to spread slowly between $t = 0$ and $tu_j / r_0 = 10$ and for $tu_j / r_0 \geq 30$, *i.e.* when the jet flow is fully laminar or fully turbulent, but more rapidly during the laminar-turbulent transitional period. In figure 5(b), the velocity decay after the potential core end at $t_c u_j / r_0 = 21.5r_0$ is fast, leading to mean centerline velocity values of $0.77u_j$ at $tu_j / r_0 = 25$ and of $0.54u_j$ at $tu_j / r_0 = 30$ for instance. This may be caused by the use of periodic conditions in the axial direction, preventing the flow scales from varying with z , hence inhibiting the entrainment of the surrounding medium in the jet. Despite this, the axial turbulence intensity increases up to a value of 20.2% at $tu_j / r_0 = 22$ in figure 5(c).

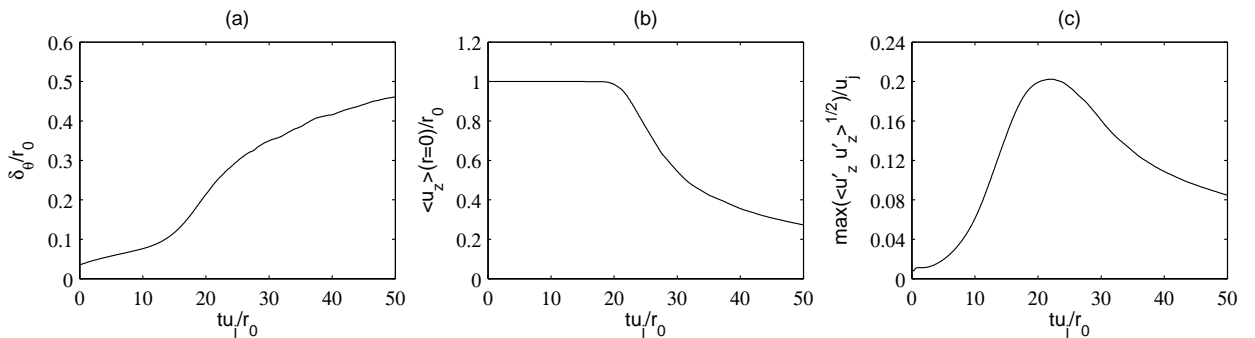


Figure 5. Time variations of (a) shear-layer momentum thickness δ_θ / r_0 , (b) mean axial velocity $\langle u_z \rangle / u_j$ at $r = 0$, and (c) the peak value of axial turbulence intensity $\langle u'_z u'_z \rangle^{1/2} / u_j$.

The time variations of the rms values and of the skewness and kurtosis factors of axial velocity fluctuations at $r = 0$ and $r = r_0$ are displayed in figure 6. In figure 6(a), as expected from figure 4(b), strong humps are obtained in both profiles of turbulence intensity, reaching maximum values of 16.7% at $tu_j/r_0 = 25$ at $r = 0$ and of 20% at $tu_j/r_0 = 21.7$ at $r = r_0$. They are due to the mergings of vortical structures³³ in the shear layers and on the jet centerline, respectively. In figures 6(b) and 6(c), significant negative values of skewness and values of kurtosis much higher than 3 are found at $r = 0$ between $tu_j/r_0 = 18$ and 25, with peak values of -1.3 at $tu_j/r_0 = 20.7$ for the skewness and of 7.8 at $tu_j/r_0 = 20.3$ for the kurtosis. This indicates intermittent occurrence of velocity deficits on the jet centerline just before the potential-core closing. They very probably follow the intrusion of shear-layer turbulent structures in the potential core of the temporal jet, as it happens at the end of the potential core of spatially-developing jets.^{8,10} At $r = r_0$, the results are quite different from those at $r = 0$. In this case, the kurtosis factor does not deviate appreciably from the value of 3, and the skewness factor is slightly positive, suggesting possible bursts of high-velocity flow structures.

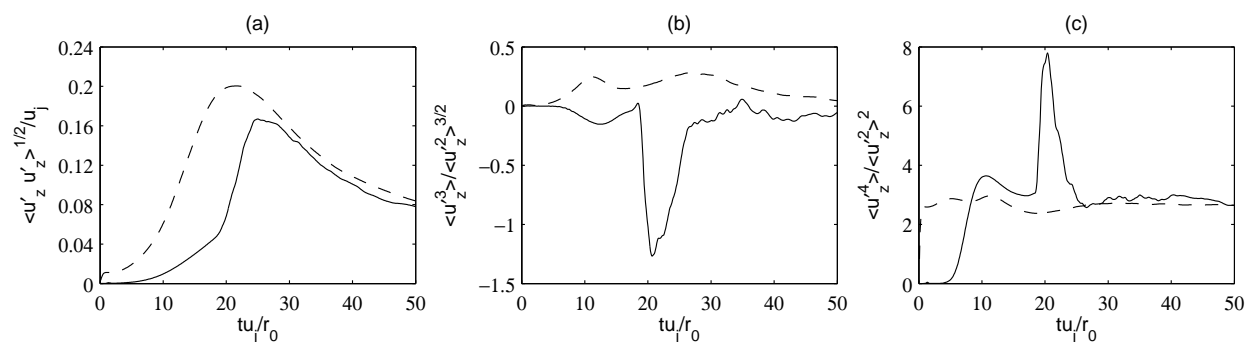


Figure 6. Time variations of the values of (a) axial turbulence intensity $\langle u'_z u'_z \rangle^{1/2} / u_j$, and (b) the skewness factor and (c) the kurtosis factor of axial velocity fluctuations u'_z at $r = 0$ and $r = r_0$.

C. Autocorrelations of flow velocity and near-field pressure

The flow and sound fields of the jet are also characterized from velocity and pressure autocorrelations. In the flow, the space-time autocorrelations of axial velocity fluctuations at radial position $r = r_1$ and time $t = t_1$ are computed in the following way

$$\mathcal{R}_{u'_z u'_z}(\delta z, \delta t) = \frac{\langle u'_z(r_1, \theta, z, t_1) u'_z(r_1, \theta, z + \delta z, t_1 + \delta t) \rangle}{\langle u'^2_z(r_1, \theta, z, t_1) \rangle^{1/2} \langle u'^2_z(r_1, \theta, z + \delta z, t_1 + \delta t) \rangle^{1/2}}$$

where δz is the spatial separation in the axial direction and δt is the time delay. The results obtained at $r = 0$ on the jet centerline at $tu_j/r_0 = 10, 20$ and 30 are represented in figure 7. The solid and dashed lines also plotted show the inclinations expected for convection velocities of $0.6u_j$ and u_j . At $tu_j/r_0 = 10$, in figure 7(a), the correlations have an oscillating shape in the axial direction, and remain significant for very large time delays. In addition, they are well aligned with the trajectory for a convection velocity of $0.6u_j$. This is not surprising given that, during the time period $1 \leq tu_j/r_0 \leq 19$ considered here, they are calculated from the instability waves growing in the jet flow. At $tu_j/r_0 = 20$, in figure 7(b), the correlations are similar to the previous ones for negative time delays, but differ for positive time delays. In the latter case, the correlations are only positive and their inclination gets closer to that corresponding to a convection velocity of u_j . This is certainly due to the arrival of turbulent structures on the centerline when the potential core closes. Finally, at $tu_j/r_0 = 30$, in figure 7(c), the correlations become less inclined with increasing time, as the jet develops and the velocity decays on the centerline.

The convection velocity u_c evaluated at $r = 0$ from the direction of the correlation spots is presented in figure 8 as a function of time. That at $r = r_0$ is also given for comparison. On the jet axis, the convection velocity increases, reaches values close to $0.86u_j$ between $tu_j/r_0 = 19.5$ and 22, and then diminishes. This is not the case at $r = r_0$, where it decreases monotonically. These results indicate that the turbulent structures that enter in the potential core just before the shear-layer merging are strongly accelerated, as in spatially-developing jets.¹⁰

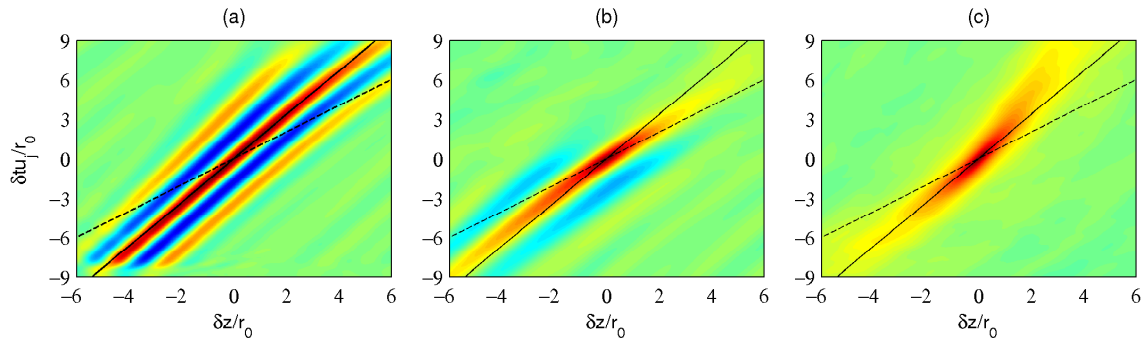


Figure 7. Representation of the space-time correlations of centerline axial velocity fluctuations at (a) $tu_j/r_0 = 10$, (b) $tu_j/r_0 = 20$ and (c) $tu_j/r_0 = 30$; — $\delta t = \delta z/(0.6u_j)$, - - - $\delta t = \delta z/u_j$. The color scale ranges from -1 to 1 .

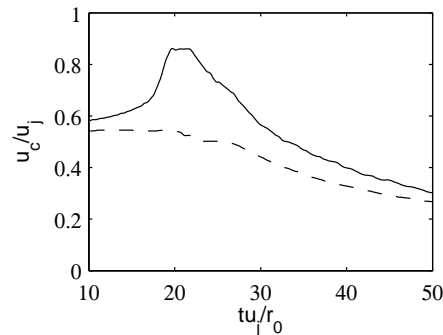


Figure 8. Time variations of the convection velocity u_c/u_j obtained from the correlations of axial velocity fluctuations at — $r = 0$ and - - - $r = r_0$.

In the jet near field, the two-dimensional spatial autocorrelations of pressure fluctuations at position $r = r_1$ and time $t = t_1$ are calculated as

$$\mathcal{R}_{p'p'}(\delta r, \delta z) = \frac{\langle p'(r_1, \theta, z, t_1)p'(r_1 + \delta r, \theta, z + \delta z, t_1) \rangle}{\langle p'^2(r_1, \theta, z, t_1) \rangle^{1/2} \langle p'^2(r_1 + \delta r, \theta, z + \delta z, t_1) \rangle^{1/2}}$$

where δr and δz are the spatial separations in the radial and axial directions. The correlations found at $r = 10r_0$ at $tu_j/r_0 = 30, 40, 50$ and 60 are shown in figure 9. As time passes, the orientation of the correlation spot changes, and indicates a direction of propagation closer to the jet direction. Its spatial extent also becomes larger. This is true along the wave front, where correlation is strong over a very large distance, but also normally to the wave front. The latter observation suggests an increase of the wavelength and thus a lowering of the frequency with time.

The radiation angle ϕ estimated from the spatial autocorrelations of pressure at $r = 10r_0$ is represented in figure 10 as a function of time. With respect to the jet direction, this angle is greater than 60° during a period centered around $tu_j/r_0 = 27.5$, when the first acoustic waves generated by the jet attain $r = 10r_0$. It then decreases with time, as expected, and falls below 30° slightly after $tu_j/r_0 = 40$ for instance.

D. Cross-correlations between flow and noise

In order to identify links between the flow and sound fields of the jet, it can be useful to compute cross-correlations between flow quantities in the jet and pressure outside, as was done in several recent experimental and numerical investigations for spatially-developing jets.^{6, 10, 50–53} Unfortunately, the flow-noise correlations calculated from the present database built from five runs of the jet simulation are not very well converged. Cross-covariances between centerline flow quantities, namely axial velocity fluctuations $u'_z, u'_z u'_z$ and vorticity fluctuations $|\omega|'$, and near-field pressure fluctuations p' at $r = 10r_0$ are however presented. For u'_z , for example, they are given by

$$\mathcal{C}_{u'_z p'}(\delta z, t_1) = \langle u'_z(r_1, \theta, z + \delta z, t_1)p'(r_2, \theta, z, t_2) \rangle$$

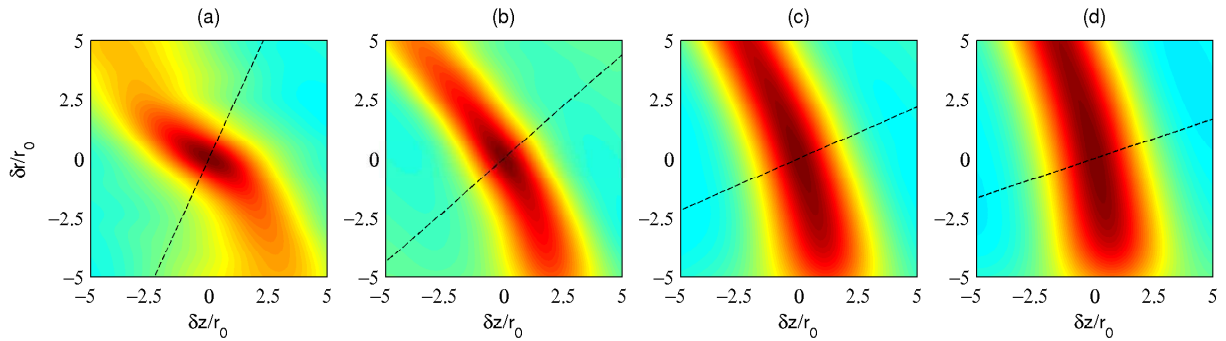


Figure 9. Representation of the 2-D spatial correlations of pressure fluctuations at $r = 10r_0$ at (a) $tu_j/r_0 = 30$, (b) $tu_j/r_0 = 40$, (c) $tu_j/r_0 = 50$ and (d) $tu_j/r_0 = 60$; - - - average direction of propagation. The color scale ranges from -1 to 1 .

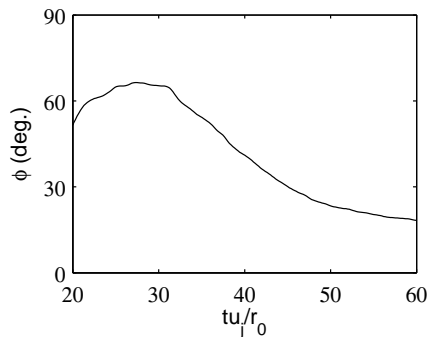


Figure 10. Time variations of the radiation angle ϕ obtained from the correlations of pressure fluctuations at $r = 10r_0$.

The flow quantities at position $(r = r_1, z + \delta z)$ at time $t = t_1$ are thus correlated with the pressure fluctuations at $(r = r_2, z)$ at $t = t_2$, with $r_1 = 0$ and $r_2 = 10r_0$ here. The cross-covariance maps obtained from pressure at $t_2 u_j/r_0 = 40$ are displayed in figure 11. High levels are found at times t_1 very close to the time of potential-core closing, represented by a dashed line. They also lie near to the solid line indicating a propagation at the ambient speed of sound between the centerline and near-field points, for negative separation distances δz . This supports the presence of a sound source on the jet axis, radiating in the downstream direction, when the shear layers merge. The correlations are moreover negative for u'_z in figure 11(a) and positive for $u'_z u'_z$ and $|\omega|'$ in figure 11(b) and 11(c). This can be related to the intermittent arrival of low-velocity turbulence structures in the jet core. Very similar results have been reported for spatially-developing jets.¹⁰

IV. Conclusion

In this paper, the flow and the near pressure fields of a temporally-developing isothermal round jet at a Mach number of 0.9 and a Reynolds number of 3125 computed by direct numerical simulations are presented. Cross-correlations between the two fields are also calculated to localize possible sound sources in the jet. It is shown, in particular, that when the jet potential core closes, vortical structures of the shear layers reach the jet centerline in an intermittent way, with a convection velocity increasing nearly up to jet initial velocity. Strong low-frequency acoustic waves are produced at the same time, and then radiate mainly in the downstream direction. Similar observations have been made at the end of the potential core of spatially-developing subsonic jets. This suggests that the sound source emitting the downstream low-frequency noise component of the latter jets is also found in temporal jets. Therefore, the existence of such a source seems not to depend on the presence of a nozzle or of a potential core of finite spatial length, or on the spatial spreading of the jet mean flow in the streamwise direction.

This original result may be somewhat unexpected, and it is hoped that it will allow us to shed new light on subsonic jet noise sources and to revisit recent theories and modellings. For the temporal jet itself, it will be interesting to better describe its flow and sound fields, notably by computing spectra, temporal and

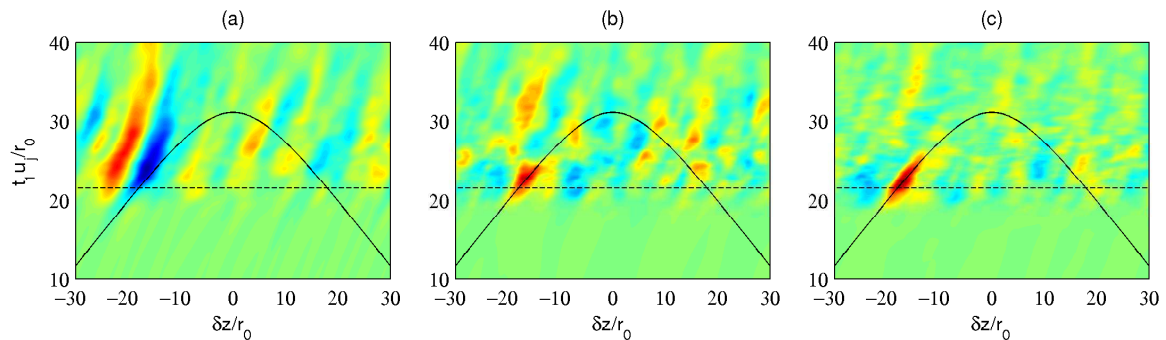


Figure 11. Space-time cross-covariances between pressure fluctuations at $r = 10r_0$ and $tu_j/r_0 = 40$ and centerline flow quantities at time t_1 : (a) axial velocity fluctuations u'_z , (b) the axial component of Reynolds stress tensor $u'_z u'_z$ and (c) vorticity fluctuations $|\omega|'$. The color scale ranges (a) from -900 to 900 Pa.m.s^{-1} , (b) -4×10^4 to $4 \times 10^4 \text{ Pa.m}^2.\text{s}^{-2}$, and (c) -8×10^7 to $8 \times 10^7 \text{ Pa.s}^{-1}$. The solid line indicates a propagation at the ambient speed of sound, and the dashed line shows the time of potential-core closing.

spatial length scales and better converged flow-noise cross-correlations. For this purpose, five additional simulations of the present jet are currently ongoing in order to perform ensemble-averaging from the results of ten runs.

Acknowledgments

This work was granted access to the HPC resources of FLMSN (Fédération Lyonnaise de Modélisation et Sciences Numériques), partner of EQUIPEX EQUIP@MESO, and of the resources of IDRIS (Institut du Développement et des Ressources en Informatique Scientifique) under the allocation 2016-2a0204 made by GENCI (Grand Equipement National de Calcul Intensif). It was performed within the framework of the Labex CeLyA of Université de Lyon, operated by the French National Research Agency (Grant No. ANR-10-LABX-0060/ANR-11-IDEX-0007).

References

- ¹Chu, W.T. and Kaplan, R.E., "Use of a spherical concave reflector for jet-noise-source distribution diagnosis," *J. Acoust. Soc. Am.*, Vol. 59, No. 6, 1976, pp. 1268-1277.
- ²Fisher, M.J., Harper-Bourne, M., and Glegg, S.A.L., "Jet engine noise source location: The polar correlation technique," *J. Sound Vib.*, Vol. 51, No. 1, 1977, pp. 23-54.
- ³Lee, S.S. and Bridges, J., "Phased-array measurements of single flow hot jets," NASA/TM 2005-213826, 2005. See also AIAA Paper 2005-2842.
- ⁴Mollo-Christensen, E., Kolpin, M.A., and Martuccelli, J.R., "Experiments on jet flows and jet noise far-field spectra and directivity patterns," *J. Fluid Mech.*, Vol. 18, 1964, pp. 285-301.
- ⁵Tam, C.K.W., "Jet noise: since 1952," *Theor. Comput. Fluid Dyn.*, Vol. 10, 1998, pp. 393-405.
- ⁶Panda, J., Seasholtz, R.G., and Elam, K.A., "Investigation of noise sources in high-speed jets via correlation measurements," *J. Fluid Mech.*, Vol. 537, 2005, pp. 349-385.
- ⁷Tam, C.K.W., Viswanathan, K., Ahuja, K.K., and Panda, J., "The sources of jet noise: experimental evidence," *J. Fluid Mech.*, Vol. 615, 2008, p. 253-292.
- ⁸Bogey, C., Bailly, C., and Juvé, D., "Noise investigation of a high subsonic, moderate Reynolds number jet using a compressible LES," *Theor. Comput. Fluid Dyn.*, Vol. 16, No. 4, 2003, pp. 273-297.
- ⁹Bogey, C. and Bailly, C., "Investigation of downstream and sideline subsonic jet noise using Large Eddy Simulations," *Theor. Comput. Fluid Dyn.*, Vol. 20, No. 1, 2006, pp. 23-40.
- ¹⁰Bogey, C. and Bailly, C., "An analysis of the correlations between the turbulent flow and the sound pressure field of subsonic jets," *J. Fluid Mech.*, Vol. 583, 2007, pp. 71-97.
- ¹¹Tam, C.K.W. and Auriault, L., "Jet mixing noise from fine-scale turbulence," *AIAA J.*, Vol. 37, No. 2, 1999, pp. 145-153.
- ¹²Tam, C.K.W. and Morris, P.J., "The radiation of sound by instability waves of a compressible plane turbulent shear layer," *J. Fluid Mech.*, Vol. 98, No. 2, 1980, pp. 349-381.
- ¹³Crighton, D.G. and Huerre, P., "Shear layer pressure fluctuations and superdirective acoustic sources," *J. Fluid Mech.*, Vol. 220, 1990, pp. 355-368.
- ¹⁴Kim, J., Moin, P., and Moser, R., "Turbulence statistics in fully developed channel flow at low Reynolds number," *J. Fluid Mech.*, Vol. 177, 1987, pp. 133-166.
- ¹⁵Eggers, J.G.M., Unger, F., Weiss, M.H., Westerweel, J., Adrian, R.J., Friedrich, R., and Nieustadt, F.T.M., "Fully

developed turbulent pipe flow: a comparison between direct numerical simulation and experiment,” *J. Fluid Mech.*, Vol. 268, 1994, pp. 175-209.

¹⁶Kozul, M., Chung, D., and Monty, J.P., “Direct numerical simulation of the incompressible temporally developing turbulent boundary layer,” *J. Fluid Mech.*, Vol. 796, 2016, pp. 437-472.

¹⁷Comte, P., Lesieur, M., and Lamballais, E., “Large- and small-scale stirring of vorticity and a passive scalar in a 3-D temporal mixing layer,” *Phys. Fluids A*, Vol. 4, No. 12, 1992, pp. 2761-2778.

¹⁸Rogers, M.M. and Moser, R.D., “Direct simulation of a self-similar turbulent mixing layer,” *Phys. Fluids*, Vol. 6, No. 2, 1994, pp. 903-923.

¹⁹Vreman, A.W., Sandham, N.D., and Luo, K.H., “Compressible mixing layer growth rate and turbulence characteristics,” *J. Fluid Mech.*, Vol. 320, 1996, pp. 235-258.

²⁰Freund, J.B., Lele, S.K. and Moin, P., “Compressibility effects in a turbulent annular mixing layer. Part 1. Turbulence and growth rate,” *J. Fluid Mech.*, Vol. 421, 2000, pp. 229-267.

²¹Freund, J.B., Lele, S.K. and Moin, P., “Compressibility effects in a turbulent annular mixing layer. Part 2. Mixing of a passive scalar,” *J. Fluid Mech.*, Vol. 421, 2000, pp. 269-292.

²²Fortuné, V., Lamballais, E., and Gervais, Y., “Noise radiated by a non-isothermal, temporal mixing layer. Part I: Direct computation and prediction using compressible DNS,” *Theor. Comput. Fluid Dyn.*, Vol. 18, No. 1, 2004, pp. 61-81.

²³Kleimann, R.R. and Freund, J.B., “The sound from mixing layers simulated with different ranges of turbulence scales,” *Phys. Fluids*, Vol. 20, No. 10, 2008, 101503.

²⁴Anderson, A.T. and Freund, J.B., “Source mechanisms of jet crackle,” AIAA Paper 2012-2251, 2012.

²⁵Buchta, D.A., Anderson, A.T., and Freund, J.B., “Near-field shocks radiated by high-speed free-shear-flow turbulence,” AIAA Paper 2014-3201, 2014.

²⁶Buchta, D.A. and Freund, J.B., “The role of large-scale structures on crackle noise,” AIAA Paper 2016-3027, 2016.

²⁷Terakado, D., Nonomura, T., Oyama, A., and Fujii, K., “Mach number dependence on sound sources in high Mach number turbulent mixing layer,” AIAA Paper 2016-3015, 2016.

²⁸van Reeuwijk, M. and Holzner, M., “The turbulence boundary of a temporal jet,” *J. Fluid Mech.*, Vol. 739, 2014, pp. 254-275.

²⁹Hawkes, E.R., Sankaran, R., Sutherland, J.C., and Chen, J.H., “Scalar mixing in direct numerical simulations of temporally evolving plane jet flames with skeletal CO/H₂ kinetics,” *Proc. Combust. Inst.*, Vol. 31, No. 1, 2007, pp. 1633-1640.

³⁰Stromberg, J.L., McLaughlin, D.K., and Troutt, T.R., “Flow field and acoustic properties of a Mach number 0.9 jet at a low Reynolds number,” *J. Sound Vib.*, Vol. 72, No. 2, 1980, pp. 159-176.

³¹Freund, J.B., “Noise sources in a low-Reynolds-number turbulent jet at Mach 0.9,” *J. Fluid Mech.*, Vol. 438, 2001, pp. 277-305.

³²Zaman, K.B.M.Q., “Effect of initial condition on subsonic jet noise,” *AIAA J.*, Vol. 23, No. 9, 1985, pp. 1370-1373.

³³Bogey, C. and Bailly, C., “Influence of nozzle-exit boundary-layer conditions on the flow and acoustic fields of initially laminar jets,” *J. Fluid Mech.*, Vol. 663, 2010, pp. 507-539.

³⁴Bogey, C., Marsden, O., and Bailly, C., “Large-Eddy Simulation of the flow and acoustic fields of a Reynolds number 10⁵ subsonic jet with tripped exit boundary layers,” *Phys. Fluids*, Vol. 23, No. 3, 2011, 035104.

³⁵Bogey, C., Marsden, O., and Bailly, C., “Influence of initial turbulence level on the flow and sound fields of a subsonic jet at a diameter-based Reynolds number of 10⁵,” *J. Fluid Mech.*, Vol. 701, 2012, pp. 352-385.

³⁶Bogey, C. and Marsden, O., “Simulations of initially highly disturbed jets with experiment-like exit boundary layers,” *AIAA J.*, **54**(4), 2016, pp. 1299-1312.

³⁷Mohseni, K. and Colonius, T., “Numerical treatment of polar coordinate singularities,” *J. Comput. Phys.*, Vol. 157, No. 2, 2000, pp. 787-795.

³⁸Bogey, C., de Cacqueray, N., and Bailly, C., “Finite differences for coarse azimuthal discretization and for reduction of effective resolution near origin of cylindrical flow equations,” *J. Comput. Phys.*, Vol. 230, No. 4, 2011, pp. 1134-1146.

³⁹Bogey, C. and Bailly, C., “A family of low dispersive and low dissipative explicit schemes for flow and noise computations,” *J. Comput. Phys.*, Vol. 194, No. 1, 2004, pp. 194-214.

⁴⁰Berland, J., Bogey, C., Marsden, O., and Bailly, C., “High-order, low dispersive and low dissipative explicit schemes for multi-scale and boundary problems,” *J. Comput. Phys.*, Vol. 224, No. 2, 2007, pp. 637-662.

⁴¹Tam, C.K.W. and Dong, Z., “Radiation and outflow boundary conditions for direct computation of acoustic and flow disturbances in a nonuniform mean flow,” *J. Comput. Acoust.*, Vol. 4, No. 2, 1996, pp. 175-201.

⁴²Bogey, C. and Bailly, C., “Three-dimensional non reflective boundary conditions for acoustic simulations: far-field formulation and validation test cases,” *Acta Acustica*, Vol. 88, No. 4, 2002, pp. 463-471.

⁴³Michalke, A., “On the inviscid instability of the hyperbolic-tangent velocity profile,” *J. Fluid Mech.*, Vol. 19, No. 4, 1964, pp. 543-556.

⁴⁴Winant, C.D. and Browand, R.K., “Vortex pairing : the mechanism of turbulent mixing-layer growth at moderate Reynolds number,” *J. Fluid Mech.*, Vol. 63, No. 2, 1974, pp. 237-255.

⁴⁵Arndt, R.E.A, Long, D.F., and Glauser, M.N., “The proper orthogonal decomposition of pressure fluctuations surrounding a turbulent jet,” *J. Fluid Mech.*, Vol. 340, 1997, pp. 1-33.

⁴⁶Coiffet, F., Jordan, P., Delville, J., Gervais, Y., and Ricaud, F., “Coherent structures in subsonic jets: a quasi-irrotational source mechanism?,” *Int. J. Aeroacoust.*, Vol. 5, No. 1, 2005, pp. 67-89.

⁴⁷Zaman, K.B.M.Q., “Flow field and near and far sound field of a subsonic jet,” *J. Sound Vib.*, Vol. 106, No. 1, 1986, p. 1-16.

⁴⁸Ukeiley, L. and Ponton, M.K., “On the near field pressure of a transonic axisymmetric jet,” *Int. J. Aeroacoust.*, Vol. 3, No. 1, 2004, pp. 43-65.

⁴⁹Bogey, C., Barré, S., Fleury, V., Bailly, C., and Juvé, D., "Experimental study of the spectral properties of near-field and far-field jet noise," *Int. J. Aeroacoust.*, Vol. 6, No. 2, 2007, pp. 73-92.

⁵⁰Panda, J., "Experimental investigation of turbulent density fluctuations and noise generation from heated jets," *J. Fluid Mech.*, Vol. 591, 2007, pp. 73-96.

⁵¹Bogey, C., Barré, S., Juvé, D., and Bailly, C., "Simulation of a hot coaxial jet : direct noise prediction and flow-acoustics correlations," *Phys. Fluids*, Vol. 21, No. 3, 2009, 035105.

⁵²Grizzi, S and Camussi, R., "Wavelet analysis of near-field pressure fluctuations generated by a subsonic jet," *J. Fluid Mech.*, Vol. 698, 2012, pp. 93-124.

⁵³Henning, A., Koop, L., and Schröder, A., "Causality correlation analysis on a cold jet by means of simultaneous Particle Image Velocimetry and microphone measurements," *J. Sound Vib.*, Vol. 332, 2013, pp. 3148-3162.